Construction and Building Materials 114 (2016) 851–863

Contents lists available at ScienceDirect

Construction and Building Materials

journal homepage: www.elsevier.com/locate/conbuildmat

Design and skid resistance evaluation of skeleton-dense epoxy asphalt mixture for steel bridge deck pavement

Zhen-dong Qian, Yang Liu *, Chang-bo Liu, Dong Zheng

Intelligent Transportation System Research Center, Southeast University, Nanjing 210096, China

HIGHLIGHTS

- One skeleton-dense epoxy asphalt mixture was designed and evaluated.
- The designed mixture meets the operating requirements of steel bridge pavement.
- The designed mixture has superior rutting resistance and anti-fatigue performance.
- The designed mixture could significantly improve the pavement skid-resistance.

ARTICLE INFO

Article history:
Received 7 December 2015
Received in revised form 16 March 2016
Accepted 29 March 2016

Keywords:
Skid-resistance
Epoxy asphalt mixture
Steel bridge deck pavement
Skeleton-dense structure
V-S volume design method

ABSTRACT

To improve the skid-resistance of epoxy asphalt concrete pavement for the steel bridge deck, an epoxy asphalt mixture with skeleton-dense structure was proposed. This paper carries out a laboratory study on the design and performance evaluation of skeleton-dense epoxy asphalt mixture. Firstly, the mixture was designed through a volume design method, and the pavement performance was investigated to evaluate the applicability of the skeleton-dense epoxy asphalt mixture for the steel bridge pavement. Secondly, the skid-resistance of the skeleton-dense epoxy asphalt mixture was evaluated, including the initial skid-resistance, long-term skid-resistance and skid-resistance under the inclement weather condition. The long-term skid-resistance attenuation law was simulated by the small traffic load simulation system MMLS3, and the skid-resistance life was predicted. The skid-resistance attenuation law under the rainy and freezing weather was investigated in the laboratory, and the influence of water film thickness, different ice situations on the pavement skid-resistance was analyzed. Finally, gray correlation analysis method was applied to the comprehensive evaluation of pavement skid-resistance. Results indicate that the proposed mixture could meet the operating requirements of steel bridge pavement and dramatically improve the skid-resistance of epoxy asphalt concrete pavement.

1. Introduction

Epoxy asphalt mixture (EAM) has been proven to be a superior material and has been widely used in the steel deck pavement [1,2]. In general, EAM is made of suspended-dense structure, which could ensure the excellent physical and mechanical properties, such as watertightness and anti-fatigue performance [1,3]. Nevertheless, the suspended-dense EAM with insufficient pavement structure depth, tends to cause the shortage of skid-resistance on the epoxy asphalt pavement, especially under the conditions of inclement weather or large longitudinal slope [3,4].

Currently, materials for skid-resistance asphalt pavement are skeleton-dense structure [5,6], which could reinforce the skid-resistance of asphalt mixture through increasing the maximum size and proportion of coarse aggregates. However, influenced by the design thickness of asphalt pavement for the steel bridge deck, the NMAS of EAM is generally restricted to 9.5 mm (the so-called EA-10). In addition, excessive coarse aggregates would sacrifice the watertightness and anti-fatigue performance of EA-10. Therefore, this paper designed the skeleton-dense EAM, to improve the skid-resistance while balancing it with the physical-mechanical properties.

The common design methods of asphalt mixture, the Marshall and SUPERPAVE design method [7,8], are mainly based on the empirical method and laboratory tests. The SUPERPAVE method is usually used for the traditional dense-graded asphalt mixture, and demands a higher level of experimental facilities and

* Corresponding author at: Intelligent Transport System Research Center, Southeast University, 35 Jingxianghe Road, Nanjing 210096, China.

E-mail addresses: qianzd@seu.edu.cn (Z.-d. Qian), seuliuyang@seu.edu.cn (Y. Liu), 243839395@qq.com (C.-b. Liu), dongzheng_seu@seu.edu.cn (D. Zheng).

http://dx.doi.org/10.1016/j.conbuildmat.2016.03.210
0950-0618/

professional skills. The Marshall method is easily performed, but the volumetric characteristics of asphalt mixture are hard to predetermine. To make the aggregates form a skeleton structure, Zhang et al. [4] developed the coarse aggregate void filling method (CAVF method), and Zhao et al. [9] developed the volume design method (V-S method) based on multi-point supported skeleton theory. The experiment processes of CAVF method and V-S method are similar to the Marshall method, and the design concept is that the coarse aggregates form the skeleton, and the fine aggregate and asphalt fill in the void of skeleton, which could ensure the good skeleton structure and waterproof performance of asphalt mixture. In the CAVF method and V-S method, the material components could be determined by calculating, but the CAVF method could only determine the proportions of coarse aggregate and fine aggregate, and the minute aggregate grading is not defined, while the V-S method proposes the minute aggregate grading design method. Therefore, the V-S design method has better practicability for the design of skeleton-dense asphalt mixture.

The objective of this study is to design the skeleton-dense EAM, to improve the skid-resistance while balancing it with the physical-mechanical properties. In this paper, the skeleton-dense EAM was designed by V-S design method, and the skid-resistance of the novel EAM was evaluated, including the initial skid-resistance, long-term skid-resistance and skid-resistance under the inclement weather condition, and gray correlation analysis was applied to evaluate the comprehensive pavement skid-resistance.

2. Design of skeleton-dense EAM

2.1. V-S design method

The V-S design method depends on the mechanical and volumetric characteristics of skeleton-dense asphalt mixture, and is comprised of three parts: coarse aggregate gradation design, fine aggregate gradation design and mixture volumetric design. The V-S design method is proposed based on the idea that coarse aggregates ($\geqslant$4.75 mm) form the skeleton of compacted mixture, fine aggregates (<4.75 mm) fill in the voids of skeleton, and asphalt binder fills in the voids of mineral aggregate, and the design equations could be presented as

$$\begin{cases} M_C + M_F = 100\% \\ \frac{M_F}{\rho_F} = \frac{M_C}{\rho_C}\left(\frac{VCA - VMA}{100}\right) \\ \frac{P_a}{\rho_a} = \left(\frac{VMA - VV}{100}\right)\frac{M_C}{\rho_C} \end{cases} \tag{1}$$

where M_C is the proportion of coarse aggregates; M_F is the proportion of fine aggregates; ρ_F is the synthesized density of fine aggregates mixed mineral powder; ρ_C and VCA are the stacking density and voids of coarse aggregates in the packing condition, respectively; VMA is the voids of the mineral aggregate; VV is air-void content of asphalt mixture; P_a is the asphalt-aggregate ratio; ρ_a is the density of asphalt binder.

In the V-S method, the volume parameters, VMA and VV, are firstly determined according to the design requirement, and ρ_F, ρ_C, ρ_a, VCA could be obtained by tests. Naturally, the rest parameters, M_C, M_F, and P_a could be calculated by Eq. (1).

According to the design concept of V-S method, the bigger aggregate particle should be densely surrounded by smaller particles, forming the multi-point supported skeleton, which could ensure the stability of aggregate skeleton, as shown in Fig. 1.

Based on the model in Fig. 1, the coarse aggregate gradation is determined as

$$V_i = \frac{V_0}{\left(1 + \frac{D_{i+1}}{D_i}\right)^3} \tag{2}$$

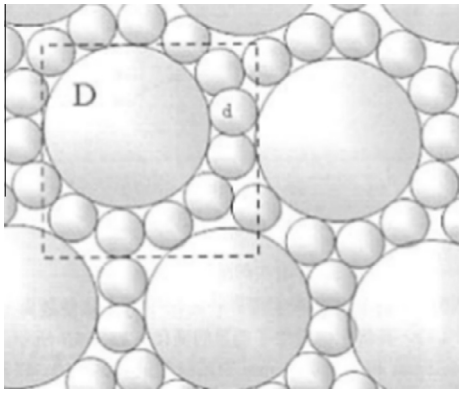

Fig. 1. Plane model of multi-point supported skeleton.

$$a_i = V_i \Big/ \sum_i V_i \tag{3}$$

where V_0 is the volume filling rate of coarse aggregates, which is defined as the bulk density divided by the apparent density of coarse aggregates [10]; V_i is the volume percent of the aggregates with the size of D_i, D_{i+1} is the aggregate with smaller size than D_i, and a_i is the volume percent of aggregates. It is noted that the volume of aggregates with the size of D_i should be deducted when calculating the volume percent of aggregates with the size of D_{i+1}.

The higher compactness of fine aggregate gradation could decrease the air-void content of asphalt mixture, and form the skeleton-dense structure of asphalt mixture. Therefore, the design of fine aggregate gradation refers to the Fuller's curve, as shown in Eq. (4)

$$P_i = (d_i/\overline{D})^n \times 100\% \tag{4}$$

where P_i is the percentage passing of aggregates with the size of d_i; $\overline{D}$ is the maximum size of fine aggregates; n is the exponent of the curve, which ranges from 0.2 to 0.45.

The procedures for the V-S design method are summarized and described below.

(1) Measure the bulk density and apparent density of coarse aggregates, and calculate the volume filling rate of coarse aggregates, V_0.
(2) Determine the coarse aggregate gradation using Eqs. (2) and (3).
(3) Determine the fine aggregate gradation using Eq. (4).
(4) Predetermine the VMA and VV of mixture, and measure the ρ_F, ρ_C, ρ_a, and VCA by the laboratory experiments, then calculate the proportion of coarse aggregates (M_C), the proportion of fine aggregates (M_F), and the asphalt-aggregate ratio (P_a) by Eq. (1).
(5) Acquire the composite gradation of mixture according to the coarse aggregate gradation, fine aggregate gradation, and the proportion of coarse aggregate and fine aggregate.

2.2. Design of VS-EA10

The EAM used in this study was mixed by basalt aggregate and epoxy asphalt binder. The technique indices of basalt aggregate and epoxy asphalt binder are list in Table 1.

The coarse aggregate gradation was determined using Eqs. (2) and (3). Because aggregate particles with the size between 2.36 mm and 4.75 mm would undermine the skeleton-dense structure of asphalt mixture [14], these particles were rejected. The design process of coarse aggregate gradation is given in Table 2.

Table 1
Technical indexes of the raw material.

Item	Technical indexes	Measured value	Criteria	Test method
Basalt aggregate	Los Angeles abrasion value (%)	11.5	⩽22.0	JTG E42-2005 [11]
	Crushing value (%)	8.9	⩽12.0	
	Acicular content (%)	1.2	⩽5	
Epoxy asphalt binder	Epoxy/asphalt ratio	1:5.85	–	ASTM D 638 [12]
	Tensile strength (23 °C, MPa)	3.26	⩾2.0	
	Fracture elongation (23 °C, %)	346	⩾200	
	Viscosity from 0 to 1 Pa·s (120 °C, min)	76	⩾50	JTG E20-2011 [13]

Table 2
Gradation of coarse aggregates.

Sieve size (mm)	V_0 (%)	Volume to be filled (%)	D_{i+1}/D_i	V_i (%)	a_i (%)
9.5	60.8	100	0.5	18.01	41.5
4.75		81.99	0.2484	25.41	58.5
1.18	–	–	–	–	–

Table 3
Gradation of fine aggregates.

Sieve size (mm)		2.36	1.18	0.6	0.3	0.15	0.075	<0.075
Percentage passing (%)	n = 0.20	100.0	87.1	76.0	66.2	57.6	50.2	–
	n = 0.25	100.0	84.1	71.0	59.7	50.2	42.2	–
	n = 0.30	100.0	81.2	66.3	53.9	43.7	35.5	–

The fine aggregate gradation was determined using Eq. (4), and the exponent n should be determined at first. The recommended range of n in the V-S method is 0.2∼0.45, but the trial calculation shows that when the value of n exceeds 0.30, the percentage passing the sieve of 0.075 mm will be down to 8.6%. Based on the research of Ma [15], the skeleton-dense asphalt mixture should control the percentage passing the sieve of 0.075 mm at about 10% to ensure the good pavement performance. Therefore, the recommended range of n is 0.2∼0.3 for designing VS-EA10. The exponent n was set as 0.2, 0.25, and 0.3 in this paper. The fine aggregate gradation is given in Table 3.

Finally, mixture volumetric design was made using Eq. (1). Based on the design requirements of EA-10 for the steel bridge deck, the *VMA* and *VV* of VS-EA10 were set as 15% and 2% respectively. ρ_F, ρ_C, ρ_a, and *VCA* were obtained by the laboratory experiments, and the proportion of coarse aggregates (M_C), the proportion of fine aggregates (M_F), and the asphalt-aggregate ratio (P_a) were calculated by Eq. (1), as shown in Table 4.

According to the calculated results in Table 4, three types of VS-EA10 were design, named VS-EA10-1 (n = 0.20), VS-EA10-2 (n = 0.25), and VS-EA10-3 (n = 0.30) respectively, and to avoid the segregation tendency of skeleton-dense asphalt mixture, 0.4% of woody fiber was added to VS-EA mixture. In addition, the EA-10 with asphalt-aggregate ratio of 6.49% and SMA-10 with asphalt-aggregate ratio of 6.40% were designed for comparison. Fig. 2 shows the gradation curves of these asphalt mixtures.

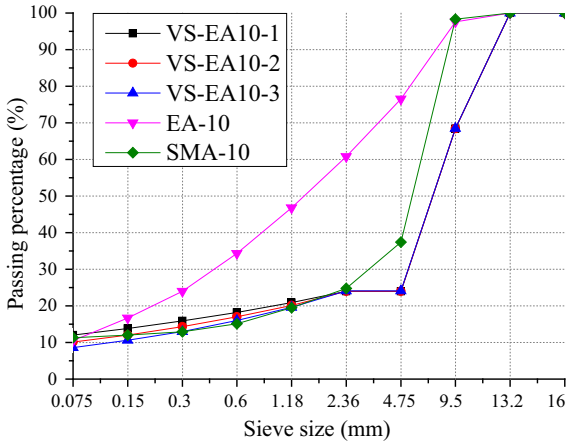

Fig. 2. Gradation curve.

3. Experiments and methods

3.1. Pavement performance

Specimens of fully cured VS-EA10, fully cured EA-10, and SMA-10 were prepared for the performance experiments, and the *VV* and *VMA* of Marshall specimens were tested firstly to verify the V-S design method. The pavement performance of VS-EA10 were evaluated to investigate its applicability for the steel bridge pavement, including the high-temperature stability, low-temperature crack resistance, moisture resistance, and anti-fatigue performance.

High-temperature stability was evaluated by dynamic stability (*DS*) measured by the slab rutting test (Fig. 3a), following a procedure in Chinese test specifications JTG E20-2011 [13]. The rutting test was conducted on the slab specimens (300 mm × 300 mm × 50 mm) at 60 °C by a solid rubber tire with a contact pressure of 0.70 MPa at a speed of 40 passes per minute for 60 min.

Low-temperature crack resistance was evaluated by the flexural strength (R_B), flexural stiffness (S_B), and flexural strain (ε_B) at failure measured by the three-point flexural beam test (Fig. 3b), following a procedure in Chinese test specifications JTG E20-2011 [13]. The beam specimens (250 mm × 30 mm × 35 mm) were loaded at a rate of 50 mm/min until failure with the test temperature at −10 °C.

Moisture resistance was evaluated by the soaked Marshall test and indirect tensile strength ratio (*TSR*) test (Fig. 3c), following procedures in Chinese test specifications JTG E20-2011 [13]. The tests were conducted on the Marshall specimens, and the *TSR* and residual Marshall stability (MS_0) were calculated.

Anti-fatigue performance was evaluated by the three-point fatigue beam test, as shown in Fig. 3(d). The test was conducted on the beam specimens (300 mm × 40 mm × 50 mm) at 15 °C, and the load control using a sinusoidal load with a 10 Hz frequency and the stress ratio was set as 0.3, 0.4, 0.5 and 0.6.

3.2. Skid-resistance

3.2.1. The initial skid-resistance

The initial skid-resistance was evaluated by the mean texture depth (MTD) measured by the sand patch method, and the British pendulum number (BPN) measured by a British Pendulum Tester (BPT). The sand patch method follows a procedure in Chinese test specifications JTG E20-2011[13] (equivalent to ASTM E 965 [16]), and the BPN was tested following a procedure in Chinese test specifications JTG E60-2008 [17] (equivalent to ASTM E 303 [18]).

The above two procedures were both conducted on the initial slab specimens (300 mm × 300 mm × 50 mm), which are prepared by the wheel rolling compactor. Prior to the BPN test, the specimen surface should be wet, and the test was

Table 4
Component proportions of VS-EA10.

	ρ_F (g/cm^3)	ρ_C (g/cm^3)	ρ_a (g/cm^3)	*VCA* (%)	M_C (%)	M_F (%)	P_a (%)
n = 0.20	2.850	1.879	1.036	35.7	76.10	23.90	6.69
n = 0.25	2.864				76.05	23.95	6.62
n = 0.30	2.876				75.93	24.07	6.56

Fig. 3. Pavement performance evaluation. (a) Rutting test (b) Three-point flexural beam test (c) Immersion Marshall Test and freeze-thaw split test (d) Three-point fatigue beam test.

Fig. 4. Skid-resistance test. (a) BPN test (b) Sand patch method.

conducted at 20 °C, as shown in Fig. 4(a). In the sand patch method, a graduate cylinder was filled with 25 mL standard sand with the particle size ranging from 0.15 mm to 0.30 mm, and the sand was spread evenly on the central area of slab specimen in a circular motion to make as flat as a pancake, and then the diameter of sand patch pancake was measured, as shown in Fig. 4b. The MTD is calculated as

$$MTD = \frac{4 \times V}{\pi \times d^2} \tag{5}$$

where V is the volume of applied standard sand, $V = 25000\text{mm}^3$; d is the diameter of sand patch pancake measured (mm).

3.2.2. The long-term skid-resistance

The initial skid-resistance could characterize the skid-resistance of newly-built pavement only, but the skid-resistance attenuation of pavements through the entire service life should also be investigated.

A third-scale Model Mobile Loading Simulator (MMLS3, as shown in Fig. 5) was used to evaluate the long-term skid-resistance of the skeleton-dense EAM. The MMLS3 is a unidirectional vehicle load simulator comprised of 4 bogies with only one pneumatic tire per bogie, these tires are 300 mm in diameter and 80 mm in width, approximately one third the diameter of a standard truck tire, as shown in Fig. 5(b). The maximum running speed of tire reaches 2.5 m/s (7200r/h), and the maximum surface contact pressure of tire approximates 0.75 MPa, and the contact load ranges from 1.9kN to 2.7kN.

In the traditional sand patch method, the standard sand is spread on the slab specimen (300 mm × 300 mm × 50 mm) as a circular pancake, therefore the traditional sand patch method is called circular sand patch method in this paper. As the width of MMLS3 groove for the specimen is less than 300 mm, specimen size of the MMLS3 test is not 300 mm × 300 mm × 50 mm (Fig. 5c). Therefore, the circular sand patch method is not eligible for the MMLS3 test, and a rectangle sand patch method was designed in this paper to measure the MTD of specimens.

In the rectangle sand patch method, the 15,710 mm^3 standard sand is spread evenly on the loading area of the specimen as a rectangle pancake, which is 80 mm in width (the same to tire width, as shown in Fig. 6a), and the length of the rectangle pancake is measured. The mean texture depth could be calculated as

$$MTD^* = \frac{V^*}{l \times d} \tag{6}$$

where MTD^* is the mean texture depth measured by the rectangle sand patch method, as opposed to the MTD measured by the circular sand patch method; V^* is the volume of applied standard sand, $V^* = 15{,}710\ \text{mm}^3$; l is the length of the rectangle pancake measured; d is the width of the rectangle pancake, $d = 80$ mm. Fig. 6 gives the graphical expression of the two sand patch method, and a comparison test of the two methods was conducted on slab specimens of different asphalt mixtures, the results were presented in Table 5. Results illustrate that the rectangle sand patch method proposed is eligible to measure the mean texture depth of asphalt mixtures.

The procedure for the MMLS3 test is illustrated by photographs in Fig. 7 and described below.

(1) Preparing the initial specimens (300 mm × 300 mm × 50 mm) by the wheel rolling compactor (Fig. 7a), the compacting temperature was 110 °C(150 °C for SMA-10 specimens) and compacting number was 36.
(2) Test specimens (300 mm × 150 mm × 50 mm) were sawn from the initial specimens (Fig. 7b). Sufficient strength should be assured before sawing to avoid the damage in surface texture.
(3) Fixing the test specimens in the test platform (Fig. 7c), and the vehicle load was simulated by the MMLS3 at 40 °C (Fig. 7d). The contact pressure and moving speed of wheel were set as 0.7 MPa and 2.5 m/s, respectively.
(4) After loading a certain number of times, lifting the equipment (Fig. 7e), and taking the specimens out to measure the BPN and MTD^* (Fig. 7f).

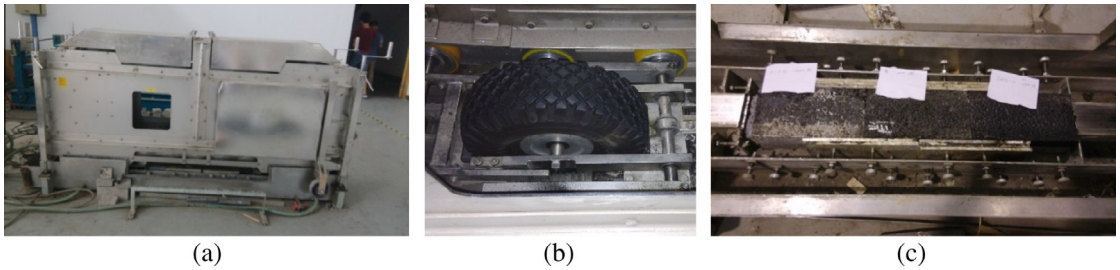

Fig. 5. MMLS3 test preparation. (a) External view (b) The one-third scale tire (c) Fixing specimens.

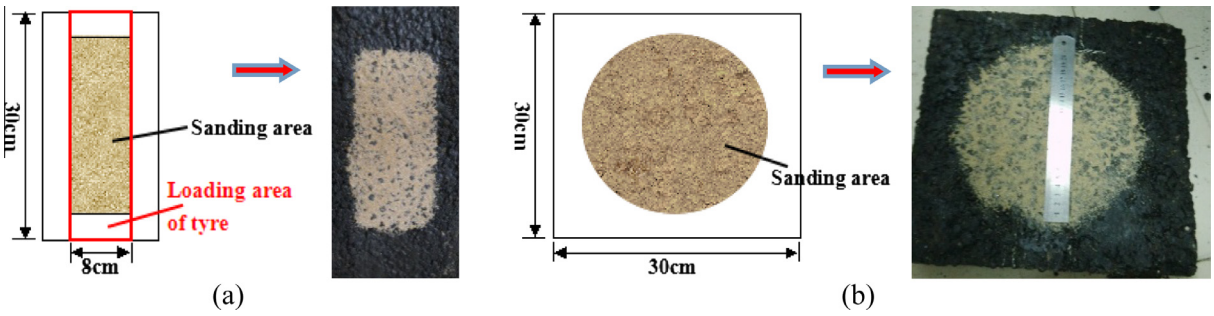

Fig. 6. Two sand patch methods. (a) Rectangle sand patch method (b) Circular sand patch method.

Table 5
MTD measured by the rectangle sand patch method and circular sand patch method.

Operation modes	MTD (mm)		
	Test 1	Test 2	Test 3
Rectangle sand patch method	0.787	0.766	0.794
Circular sand patch method	0.795	0.757	0.788

(5) Repeating step(3) and step(4) until the end of test. This study set the loading times as 300,000 times, because the BPN and MTD* of VS-EA10 and EA-10 specimens tend to stabilize after loading 300,000 times, while apparent deformation will emerge on the SMA-10 specimens when loading 300,000 times.

3.2.3. The skid-resistance under the inclement weather condition

The tire-pavement skid-resistance was determined by the surface texture characteristics of pavement and tire, and the interfacial medium between the tire and pavement [19]. Under the inclement weather condition, such as the rainy and freezing weather, contaminants (water, ice) can invade the interfacial medium, threatening the driving safety [20].

In this section, two inclement conditions were simulated in the laboratory. The slab specimens (300 mm × 300 mm × 50 mm) were used to simplify the pavement, and the area of 200 mm × 250 mm on the slab specimens, which was called simulation area, was used to simulate the surface texture characteristics of pavement under different inclement weather conditions, as shown in Fig. 8. The skid-resistance was evaluated by the British pendulum number measured by the British Pendulum Tester. Due to the research objective in this section, the specimens should not to be wet before measuring the British pendulum number (abbreviated as BPN*).

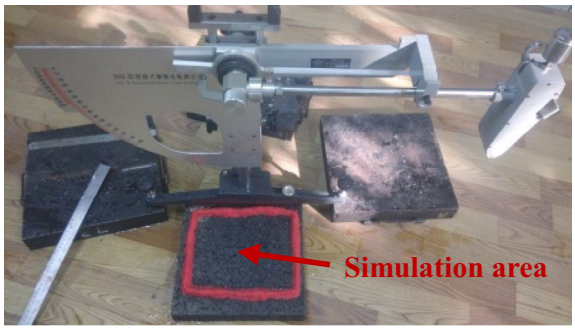

Fig. 8. Simulation area on the slab specimen.

During a rainy period, water film is formed between the tire and pavement, leading to a lack of tire-pavement skid-resistance. The water film thickness is different at different stages, and the skid-resistance of pavement is also different. Therefore, the effect of water film thickness on the pavement skid-resistance was studied. The test process was described below.

(1) Encircling the simulation area with the waterproof material, in case the water flows away, as shown in Fig. 8.
(2) Spraying a certain volume of water on the simulation area with a sprinkling can, the mean water film thickness was decided by the water quantity sprayed on the slab specimen, as shown in Table 6. Subsequently, measuring the BPN* and drying the specimen with a warm air blower before the next measurement.

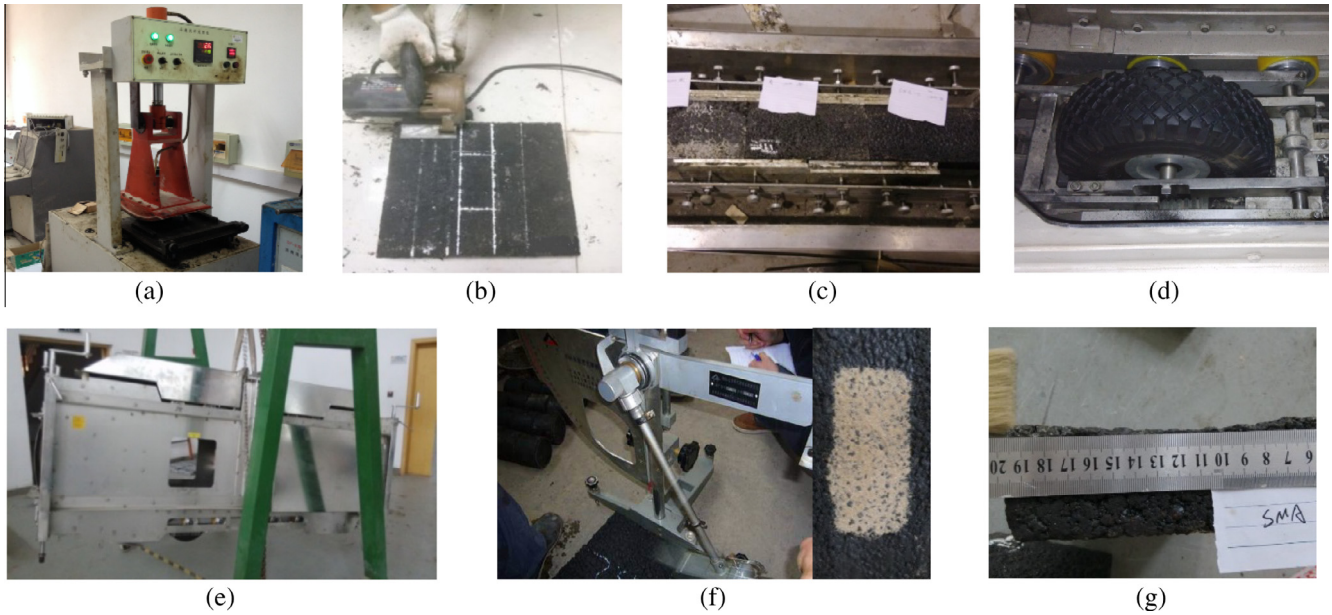

Fig. 7. The general procedure for the research of long-term skid resistance.

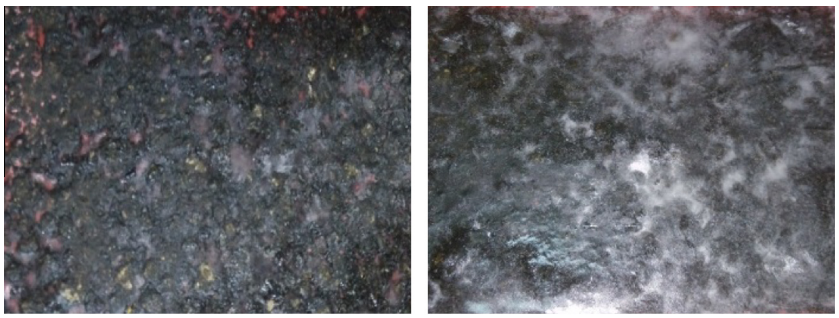

Fig. 9. Two kinds of icy pavement. (a) Partial-covered (b) All-covered.

Table 6
Water quantities for different water film thickness.

Thickness (mm)	0.03	0.05	0.10	0.25	0.50	1.00	2.00
Water quantity (mL)	1.5	2.5	5	12.5	25	50	100

Different ice situations on the pavement were simulated. Three expressions as None-covered, partial-covered, and all-covered were used to describe the ice situations on the pavement. The none-covered situation means that the simulation area is clean, and the partial-covered situation means that part of the simulation area is covered by contaminants, and the all-covered situation means that the entire simulation area is covered by contaminants. The detailed process was illustrated in Table 7 and described below.

(1) Soaking the slab specimen in the 25 °C water for 24 h until water-saturated state.
(2) Taking out the specimen, and drying the specimen surface.
(3) Spraying a certain volume of water (Table 7) on the specimen, and putting the specimen into the −18 °C cryogenic box for 16 h.
(4) Taking out the specimen, and continuously measuring the BPN* until the ice fully melt.

4. Results and discussion

4.1. Pavement Performance

The volumetric parameters and pavement performances of VS-EA10, EA-10 and SMA-10 were given in Table 8 and Fig. 10.

As shown in Table 8, the VV and VMA of VS-EA10 obtained by tests agree well with the predetermined VV (2.0%) and VMA (15%). This indicates that the V-S method could design VS-EA10 with the desired volumetric parameters.

The mean *DS* of three VS-EA10 is 21267 passes per millimeter, which is slightly higher than EA-10 and approximately triples the *DS* of SMA-10. This is primarily due to the thermosetting property of epoxy asphalt, which does not soften as the conventional asphalt at high temperature. In addition, the skeleton structure could boost the high-temperature stability to some extent.

Table 7
Detailed information of two kinds of icy pavement specimens.

Ice situations	Water volume	Features	Simulated road conditions
Partial-covered	15 mL	Partial aggregates are exposed, ice exists among aggregates (Fig. 9a).	The road is icy after raining
All-covered	50 mL	The specimen is covered by ice completely (Fig. 9b).	Snow accumulates on the road after continuous raining and snowing

As can be observed in Table 8, the VS-EA10 has the highest flexural strength (R_B) at low temperature (−10 °C), but the mean flexural strain (ε_B) of VS-EA10 at low temperature (−10 °C) is 2.63×10^{-3}, which is slightly higher than the minimum value (2.50×10^{-3}) typically required for the steel bridge deck pavement. This is due to the higher content of coarse aggregates in VS-EA10, and cracks are liable to generated along the coarse aggregate during the bending. Once the crack occurs, it will extend faster in the VS-EA10, resulting in the lower flexural strain.

The *TSR* and MS_0 values of VS-EA are both around 90%, which is higher than the minimum values (85%) typically required for the steel bridge deck pavement. Comparing the *TSR* and MS_0 of VS-EA10 with that of EA-10, the moisture resistance of VS-EA10 is inferior to EA-10 despite the similar VV value. This indicates that the voids and cracks in VS-EA10 are liable to form the penetrated channel in the specimen, which could enhance the moisture effect.

As shown in Fig. 10, the fatigue life of VS-EA10 is inferior to that of EA-10, indicating that the increase of coarse aggregates could decrease the fatigue life of asphalt mixture. However, the fatigue life of VS-EA10 is superior to SMA-10, although the coarse aggregate content in VS-EA10 is higher than that of SMA-10. This indicates that the effect of air-void content on the anti-fatigue performance of asphalt mixture is more than the effect of coarse aggregate content.

In conclusion, the designed VS-EA10 could meet the operating requirements of steel bridge pavement, and the pavement performance differences among VS-EA10-1, VS-EA10-2 and VE-EA10-3 are unapparent, but the deformability of VS-EA10 at low temperature needs to be improved.

4.2. Skid-resistance

4.2.1. The initial skid-resistance

To evaluate initial skid-resistance of VS-EA10, EA-10 and SMA-10, the MTD and BPN values of initial specimens were measured. The results are summarized in Table 9. It is recognized that insufficient MTD value leads to the shortage of skid-resistance in EAM. As can be seen in Table 9, the mean MTD value of VS-EA10 is 0.97 mm, which is superior to SMA-10 and is about four times higher than EA-10. All the BPN values of VS-EA10, EA-10 and SMA-10 are around 65, which are significantly larger than the minimum value (45) typically required for the steel bridge deck pavement. Therefore, it could be concluded that the designed VS-EA10 could vastly increase the initial skid-resistance of EAM. In addition, comparison of the MTD and BPN values of the three VS-EA10 reveals that VS-EA10-3 has the first-rank initial skid-resistance.

4.2.2. The long-term skid-resistance

To determine the relationship between skid-resistance and load repetitions, the measured BPN and MTD values at different load

Table 8
Volumetric parameters and pavement performances of VS-EA10, EA-10, and SMA-10.

Technical indexes	VV/%	VMA/%	High-temperature stability	Low-temperature crack resistance			Moisture susceptibility	
			DS/(mm^{-1})	R_B/MPa	ε_B/10^{-3}	S_B/MPa	TSR/%	MS_0/%
VS-EA10-1	1.6	16.3	22,000	27.13	2.53	10879	90.5	91.8
VS-EA10-2	2.1	16.5	21,200	24.49	2.86	9323	92.7	89.5
VS-EA10-3	2.4	16.7	20,600	26.87	2.51	10700	89.7	92.8
EA-10	1.9	16.5	18,000	24.18	3.72	6500	96.8	98.2
SMA-10	3.0	17.3	7007	10.31	3.09	3337	88.3	91.3
Criteria*	1.0 ~ 3.0	–	⩾8000	–	⩾2.50	–	⩾85	⩾85

* Index criteria for the steel bridge deck pavement, and the same below.

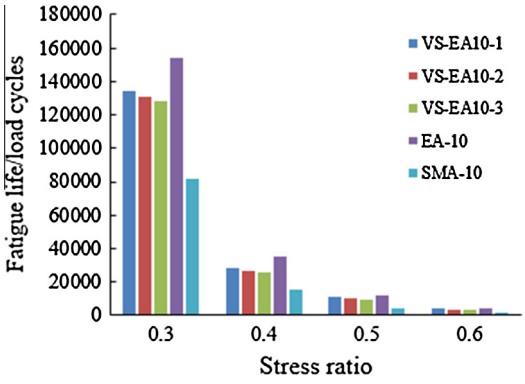

Fig. 10. Fatigue life of VS-EA10, EA-10, and SMA-10 at different stress ratios.

Table 9
Test results of skid resistance property.

Asphalt mixture types	MTD/mm	BPN
VS-EA10-1	0.88	66
VS-EA10-2	0.98	62
VS-EA10-3	1.04	76
EA-10	0.21	65
SMA-10	0.84	67
Criteria	⩾0.55	⩾45

repetitions are shown in Fig. 11. As shown in Fig. 11(a), the skid-resistance of VS-EA10 is superior during the entire load cycle, and the BPN values change in three phases with load repetitions [21]. In the coarsening phase, with the bitumen coating on the top of aggregates being removed by the tire, the BPN values increase in the first instance. After a complete removal of the bitumen coating, the BPN values decrease due to the polishing of aggregates (the polishing phase), until stabilize at a low BPN value in the equilibrium phase. As shown in Fig. 11(b), the MTD values of EA-10 hardly change with load repetitions, and the MTD values of VS-EA10 and SMA-10 see a downward trend. In addition, the MTD values of SMA-10 at different load repetitions could also be defined as three phases: the compacting phase, the polishing phase, and the equilibrium phase. In the compacting phase, the SMA-10 specimen is compacted by the wheel load, resulting in the decrease of MTD values. After a complete compaction, the MTD values of SMA-10 carry on decreasing due to the polishing of coarse aggregates (the polishing phase), but the decrease rate in this phase is lower than the compacting phase. Finally, the MTD values stabilize in an equilibrium phase. Due to the density of VS-EA10 and EA-10, the initial compacting process is not observed in the VS-EA10 specimens, and the MTD values vary in two phases (the polishing phase, the equilibrium phase).

The BPN test and MTD test could estimate the pavement skid-resistance at different circumstances. To harmonize the two test, the International Friction Index (IFI) [22] was used to make a comprehensive evaluation on the skid-resistance of mixture, and the skid-resistance life was predicted by the IFI values.

The IFI contain two parameters: F_{60} and S_P, the calculation of the IFI is as follow:

$$S_P = a + bT_x \tag{7}$$

$$F_{60} = A + B \cdot FRS \cdot \exp[(S - 60)/(a + bT_x)] \tag{8}$$

where S_P is the texture parameter of IFI; F_{60} is the friction parameter of IFI; T_x is the macrotexture parameter of pavement, equivalent to the MTD in this research; a, b, A and B are empirically determined

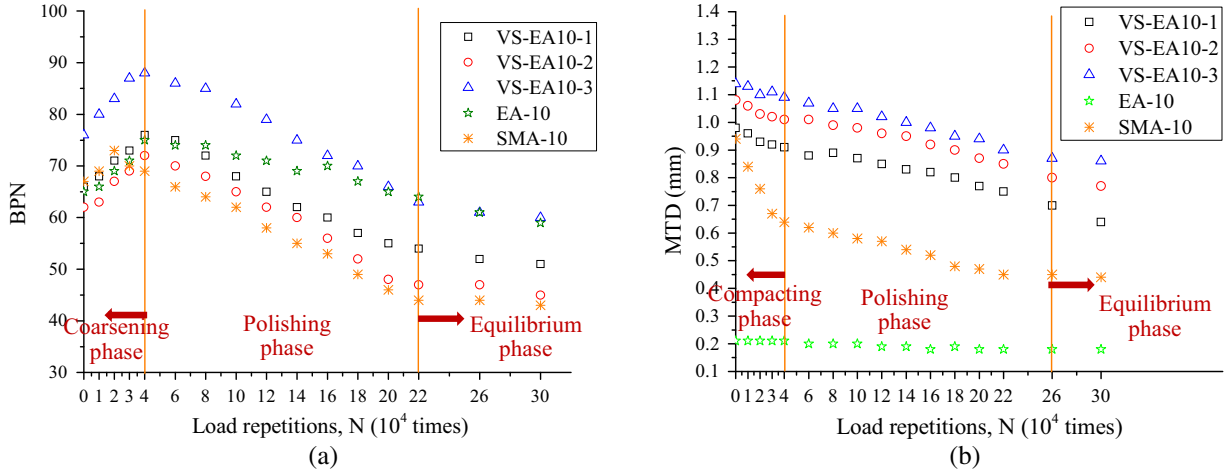

Fig. 11. Changes of skid-resistance with load repetitions. (a) Measured BPN values (b) Measured MTD values.

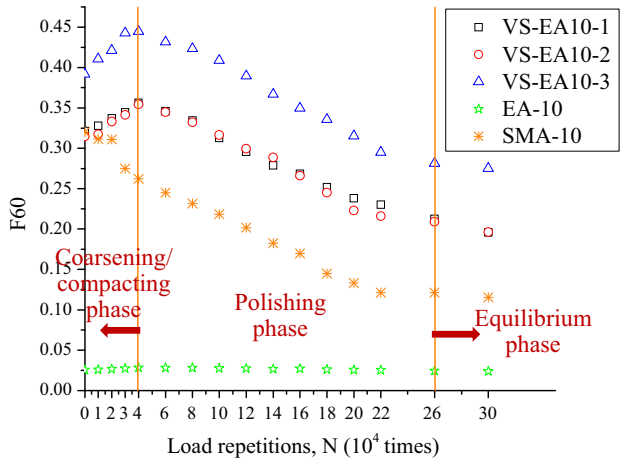

Fig. 12. F_{60} changes with load repetitions.

coefficients, a = -11.5981, b = 113.63426, A = 0.07784, B = 0.00709 [23]; S is the slip speed, which was defined as the swing speed of British Pendulum Tester, S = 10 km/h; *FRS* is defined as the BPN value measured at speed S.

As can be seen in Eqs. (7) and (8), F_{60} is related with MTD and BPN, while S_p is only decided by MTD. Therefore, F_{60} could well harmonize the BPN test and MTD test. The F_{60} values of different asphalt mixtures under different load repetitions were calculated by Eq. (8), as shown in Fig. 12. The mean F_{60} of EA-10 is around 0.028, indicating the insufficient skid-resistance. The F_{60} values of VS-EA10 and SMA-10 at different load repetitions could be distributed into three phases as well, but the change regularity of F_{60} values in the first phase is different. In the first phase, the coarsening process occurs on the VS-EA10 specimen, resulting in the increase of F_{60} values of VS-EA10. While in the SMA-10 specimen, the coarsening process and compacting process are both occurred in the first phase. The former process could increase the F_{60} value, but the latter process decrease the F_{60} value. Therefore, it is observed that the F_{60} value of SMA-10 decreases with a low rate in the first phase.

Based on the calculated F_{60} values, the relationship between the skid-resistance and load repetitions could be determined. To establish the change regularity of F_{60} with load repetitions, N ($\times 10^4$ times) accurately, the F_{60} values in the first phase were abandoned. The fitting curves and fitting equations of F_{60} with load repetition, N ($\geqslant 4 \times 10^4$ times) are given in Fig. 13 and Table 10, respectively.

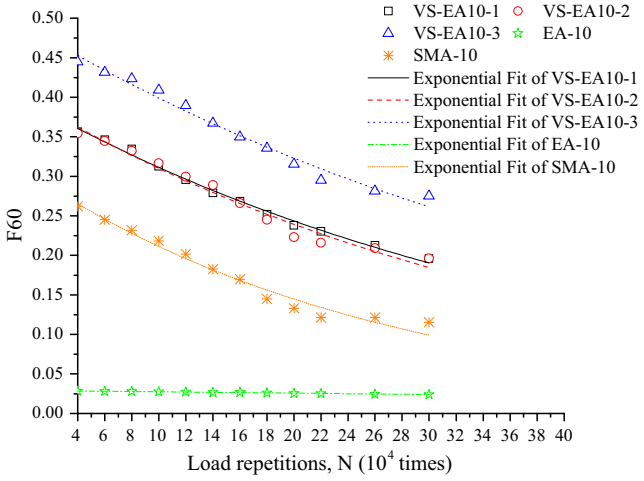

Fig. 13. Fitting curves of *F*60 with load repetitions, N ($\times 10^4$ times).

Prior to predicting the skid-resistance life of VS-EA10, the threshold value of F_{60} should be defined. The threshold value was defined in three steps according to the threshold values of BPN and MTD for the steel bridge deck pavement (BPN $\geqslant$ 45, MTD $\geqslant$ 0.55 mm).

(1) Establishing the relationships between BPN, MTD values and load repetitions, N ($\geqslant 4 \times 10^4$ times). The fitting curves and fitting equations are given in Fig. 14 and Table 11, respectively.
(2) Calculating the skid-resistance life based on the threshold values of BPN (45) and MTD (0.55 mm), the results are calculated in Table 11.
(3) SMA-10 is a typical skid-resistance material for the steel bridge deck surfacing. Therefore, the threshold value of F_{60} was decided according to the skid-resistance life of SMA-10. As can be seen in Table 11, the skid-resistance life of SMA-10 is 12.84×10^4 times load repetitions, and the corresponding F_{60} value was 0.192 (calculated by the equation in Table 10). Hence the threshold value of F_{60} for the steel bridge deck pavement is defined as 0.192.

The skid-resistance life of three VS-EA10 were calculated based on the threshold value of F_{60}, the results were summarized in Table 12. The skid-resistance life of VS-EA10 is far longer than SMA-10, concluding that the skid-resistance durability of VS-EA10 is superior. Comparing the skid-resistance life amongst the three VS-EA10, VS-EA10-3 has the longest skid-resistance life, then followed VS-EA10-1 and VS-EA10-2.

4.2.3. The skid-resistance under the inclement weather condition

4.2.3.1. Effect of water film thickness on the pavement skid-resistance. To evaluate the effect of water film thickness on the skid-resistance of VS-EA10, EA-10 and SMA-10, the BPN* values of these asphalt mixture pavements with different water film thickness were shown in Fig. 15. The BPN* values of these asphalt mixture see a downward trend with the increase of water film thickness, and the change of BPN* values could be divided into three phases based on the descend rate. In the wetting phase (water film thickness $\leqslant$ 0.1 mm), the pavement surface changes from dry state to wet state, but there is no accumulated water on the surface, as shown in Fig. 16(a). In this phase, the BPN* values drop dramatically because the water fills the gap between asperities on the pavement surface, decreasing the contact area between the rubber block of BPT and the pavement, and reducing the adhesion between the rubber block of BPT and the pavement. With the increase of water film thickness, the accumulated water appears on the pavement (Fig. 16b), and dynamic water will form during the relatively slip between the rubber block and the pavement, which play a lubrication role, leading to the BPN* values drop continuously in the partial accumulated water phase (0.1 mm $\leqslant$ water film thickness $\leqslant$ 1 mm). However, when the water film thickness exceed 1 mm, the pavement surfaces are totally covered by water, as shown in Fig. 16(c). In the total accumulated water phase (water film thickness $\geqslant$ 1 mm), the lubrication effect of the dynamic water reaches the peak, and the hydroplaning phenomenon would occur during the relatively slip between the rubber block and the pavement, therefore the BPN* stabilizes at the minimum value.

As shown in Fig. 15, the water film thickness boundaries of different phases are the 0.1 mm and 1 mm. To compare the skid-resistance of different asphalt mixture pavements under the rainy condition, the BPN* values of different asphalt mixture pavements under the water film thickness of 0.1 mm and 1 mm are summarized in Fig. 17. It can be observed that the skid-resistance of VS-EA10-1 and VS-EA10-2 under the rainy condition are comparable to that of SMA-10, and are slightly better than that of EA-10. The

Table 10
Fitting equation of $F60$ with N ($\times 10^4$ times).

	VS-EA10-1	VS-EA10-2	VS-EA10-3	EA-10	SMA-10
Fitting equation	$F60 = 0.396e^{-0.024N}$ (N ⩾ 4)	$F60 = 0.400e^{-0.026N}$ (N ⩾ 4)	$F60 = 0.491e^{-0.021N}$ (N ⩾ 4)	$F60 = 0.029e^{-0.007N}$ (N ⩾ 4)	$F60 = 0.313e^{-0.038N}$ (N ⩾ 4)
R^2	0.9941	0.9691	0.9774	0.9832	0.9698

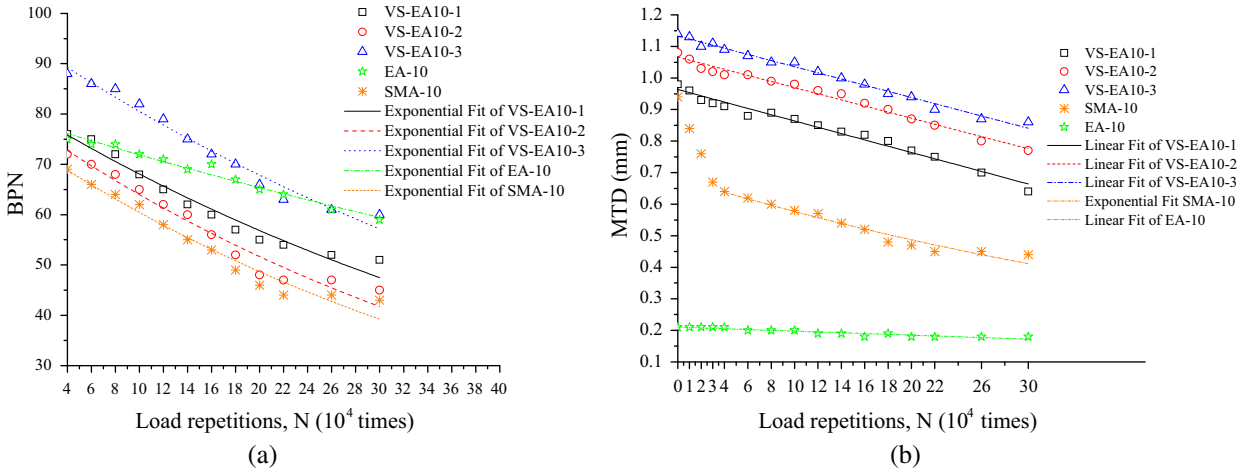

Fig. 14. Fitting curves of BPN and MTD with loading times, N. (a) BPN (b) MTD.

Table 11
Fitting results of BPN and MTD with loading times, N ($\times 10^4$ times).

Asphalt mixture types	BPN		MTD	
	Fitting equation	Skid-resistance life /$\times 10^4$ times	Fitting equation	Skid-resistance life /$\times 10^4$ times
VS-EA10-1	$BPN = 80.56e^{-0.017N}$	34.25	$MTD = 0.964\text{-}0.010N$	41.36
VS-EA10-2	$BPN = 78.45e^{-0.021N}$	26.47	$MTD = 1.066\text{-}0.010N$	53.22
VS-EA10-3	$BPN = 95.24e^{-0.017N}$	44.10	$MTD = 1.133\text{-}0.010N$	59.52
EA-10	$BPN = 79.22e^{-0.010N}$	56.55	$MTD = 0.21$	–
SMA-10	$BPN = 74.05e^{-0.021N}$	23.72	$MTD = 0.684e^{-0.017N}$	12.84

Table 12
Skid-resistance life of VS-EA10.

Asphalt mixture types	Forecasting equation	Skid-resistance life ($\times 10^4$ times)
VS-EA10-1	$F60 = 0.396e^{-0.024N}$ (N ⩾ 4)	30.38
VS-EA10-2	$F60 = 0.400e^{-0.026N}$ (N ⩾ 4)	28.38
VS-EA10-3	$F60 = 0.491e^{-0.021N}$ (N ⩾ 4)	45.00

VS-EA10-3 shows a superior skid-resistance under the rainy condition, and the BPN* value of VS-EA10-3 in the total accumulated water phase could reach 75, even more than the BPN* values of other asphalt mixtures in the wetting phase. Therefore, it could be concluded that the VS-EA10 with reasonable aggregate gradation could improve the skid-resistance of steel bridge deck pavement under the rainy condition.

The evaluation of skid-resistance of asphalt mixture pavement under the inclement weather is not only to evaluate the BPN* values, but also the skid-resistance attenuation. This research defined the skid-resistance attenuation percentage of pavement under different water film thickness, F as follow:

$$F_i = \frac{BPN^*_{max} - BPN^*_i}{BPN^*_{max}} \quad (9)$$

where F_i is the skid-resistance attenuation percentage of pavement under the water film thickness of i; BPN^*_{max} is the BPN* value of pavement under the dry condition; BPN^*_i is the BPN* value of pavement under the water film thickness of i.

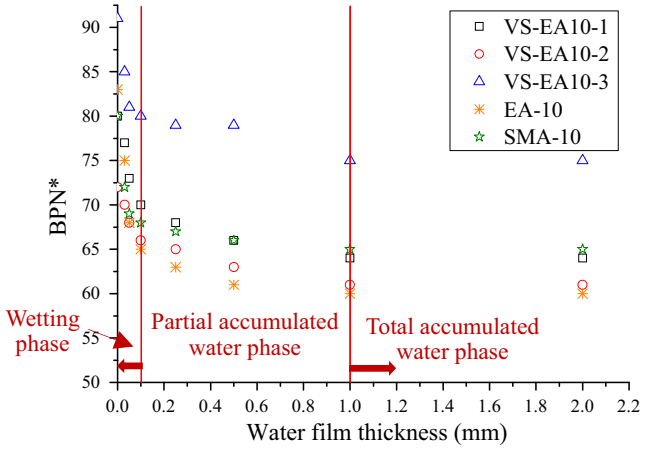

Fig. 15. BPN* values change with different water film thickness.

To evaluate the skid-resistance attenuation of different asphalt mixtures, the $F_{0.1mm}$ and F_{1mm} of asphalt mixtures were calculated, as shown in Fig. 18. It can be seen that the skid-resistance attenuations of EA-10 are much more than SMA-10, that is why the skid-resistance of EA-10 under the rainy condition is inferior to SMA-10,

Fig. 16. The pavement surface conditions in three phases. (a) Wetting phase (b) Partial accumulated water phase (c) Total accumulated water phase.

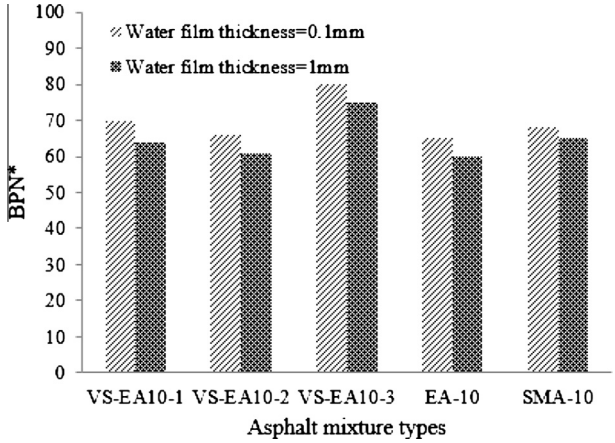

Fig. 17. BPN* of different mixtures.

although the BPN* values of them are almost the same (as shown in Fig. 17). In addition, it could also been observed that the skid-resistance attenuations of VS-EA10 are slightly better than that of SMA-10, and much better than that of EA-10. Combined with the BPN* analysis of asphalt mixtures under the different water film thickness in Fig. 17, it could be concluded that the VS-EA10 pavement could ensure the sufficient skid-resistance in the rainy day.

4.2.3.2. Effect of ice situations on the pavement skid-resistance. To evaluate the skid-resistance of VS-EA10, EA-10 and SMA-10 pavements under the partial-covered and all-covered ice situations, the BPN* values of these pavement specimens were continuously measured until the ice fully melt. The results are summarized in Fig. 19,

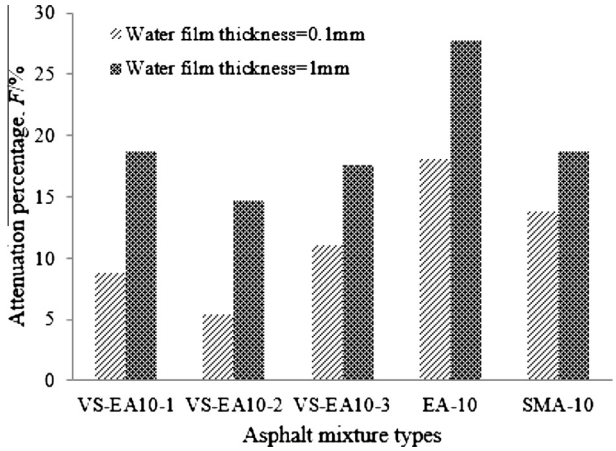

Fig. 18. Attenuation percentage of different mixtures.

and it can be seen that the effect of ice situations on the pavement skid-resistance shows obvious differences in different stages.

As shown in Fig. 19(a), the change of BPN* under the partial-covered ice situation could be divided into three phases. It can be seen that the BPN* experiences a downward trend first and then rises, until remains stable when the ice is fully melt, and the pavement under the partial-covered ice situation also experienced three conditions, as shown in Fig. 20. Therefore, this research named the three change phases of BPN* under the partial-covered ice situation as ice phase, ice-water mixed phase and accumulated water phase respectively.

As shown in Fig. 19(b), the change of BPN* under the all-covered ice situation could be divided into four phases. It can be seen that the BPN* experiences a downward trend in the first phase, and then stabilizes at the lowest point. After that, the BPN* rises in the third phase until remains stable when the ice is fully melt. Similarly, the pavement under the all-covered ice situation experienced four conditions, as shown in Fig. 21. Therefore, this research named the three change phases of BPN* under the partial-covered ice situation as ice phase, ice membrane phase, ice-water mixed phase and accumulated water phase respectively.

To evaluate the skid-resistance of VS-EA10, EA-10 and SMA-10 pavements in the freezing day, the minimum BPN* values and the skid-resistance attenuations of these asphalt mixtures are investigated. Because the minimum BPN* values of these asphalt mixtures under the all-covered ice situation are below 30, and the pavement condition does not meet the driving requirement, therefore, it is not necessary to analyze the minimum BPN* values under the all-covered ice situation. Fig. 22 gives the minimum BPN* values under the partial-covered ice situation, it can be seen that the minimum skid-resistance of VS-EA10 and SMA-10 is superior to that of EA-10. This indicates that the skeleton-dense asphalt mixture has the better pavement skid-resistance in the freezing day.

To evaluate the skid-resistance attenuations of VS-EA10, EA-10 and SMA-10, this research defined the skid-resistance attenuation percentage of pavement under the ice situation, P as follow:

$$P = \frac{BPN^*_{max} - BPN^*_{ini}}{BPN^*_{max}} \tag{10}$$

where BPN^*_{max} is the BPN* value of pavement under the dry condition; BPN^*_{ini} is the initial BPN* value of pavement in each phase.

Fig. 23 gives the skid-resistance attenuation percentages of pavements under the partial-covered ice situation and the all-covered ice situation. It can be seen that the skid-resistance attenuation regularity of pavements under different ice situations are similar. The skid-resistance attenuations of VS-EA10 and SMA-10 are better than that of EA-10, and the skid-resistance of VS-EA10-3 has the least attenuation in every phase. Therefore, it could be concluded that the VS-EA10 could improve the skid-resistance of steel bridge deck pavement in the freezing day.

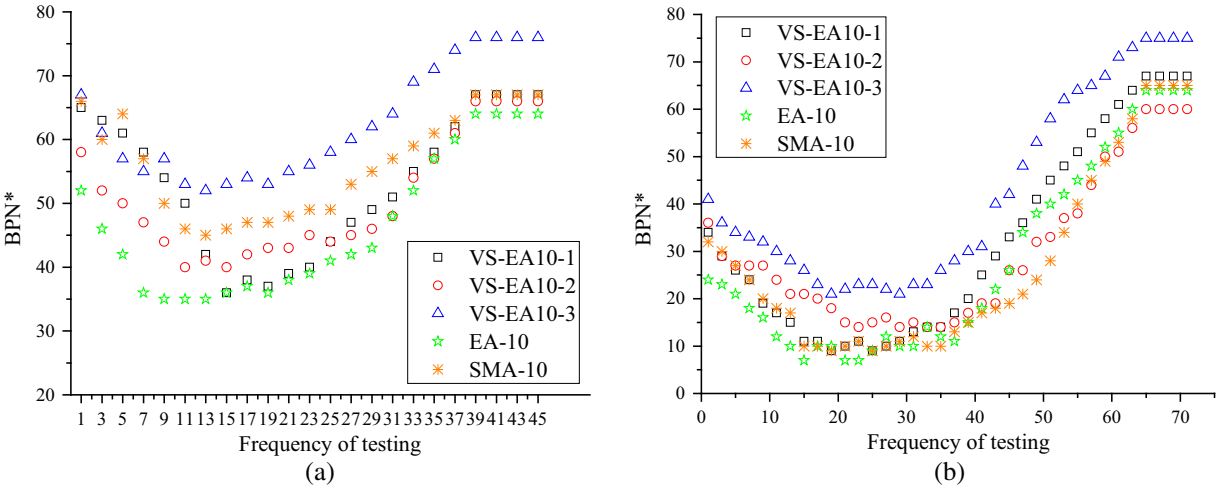

Fig. 19. The BPN* change regularity under different ice situations. (a) Partial-covered (b) All-covered.

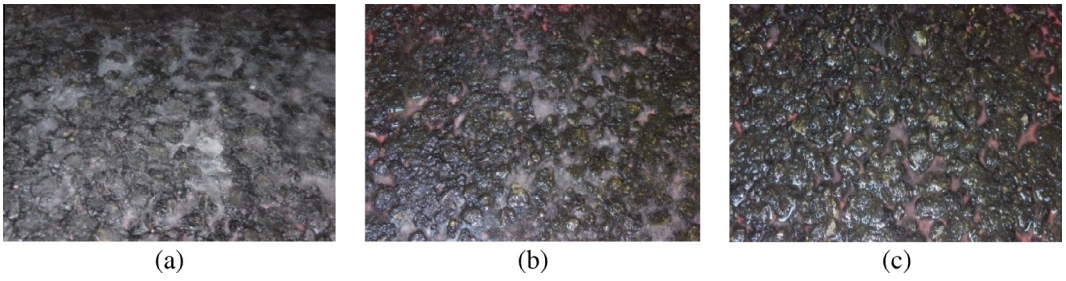

Fig. 20. Pavement conditions under the partial-covered ice situation. (a) Ice (b) Ice-water mixed (c) Accumulated water.

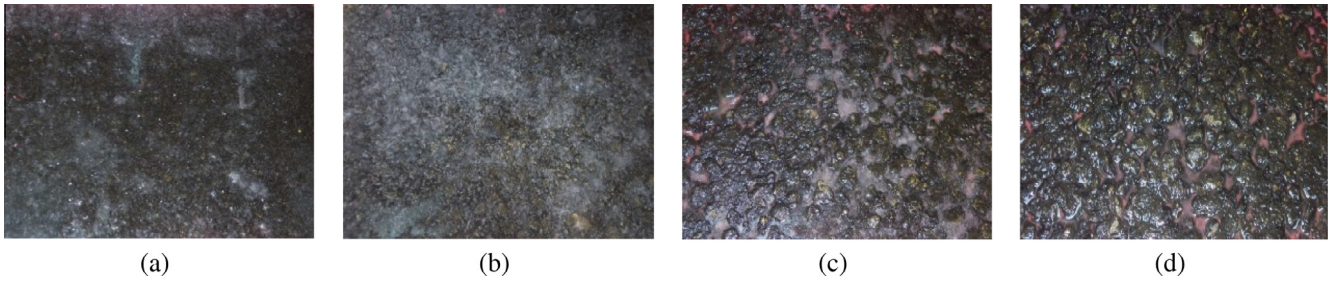

Fig. 21. Pavement conditions under the all-covered ice situation. (a) Ice (b) Ice membrane (c) Ice-water mixed (d) Accumulated water.

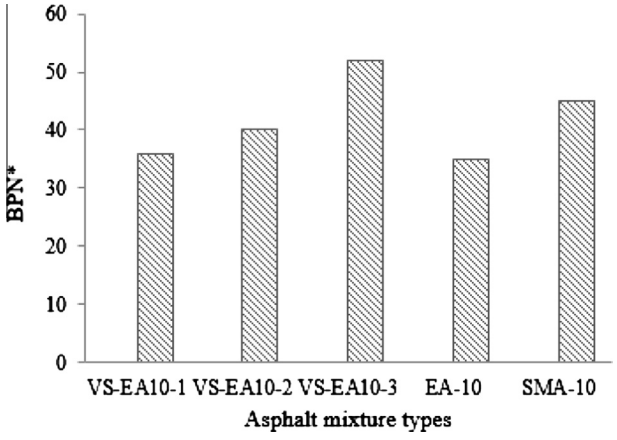

Fig. 22. The minimum BPN* values under the partial-covered ice situation.

4.2.4. The comprehensive evaluation of skid-resistance based on gray correlation analysis

Definitely, the evaluation of pavement skid-resistance should synthesize the initial skid-resistance, long-term skid-resistance and the skid-resistance under the inclement weather condition, which involves the multi-index comparison and analysis. In this section, the gray correlation analysis was applied to evaluate comprehensive skid-resistance of VS-EA10-1, VS-EA10-2, VS-EA10-3, EA-10 and SMA-10.

First of all, the skid-resistance evaluation indicators should be determined. This research chose BPN and MTD as the evaluation indicators for the initial skid-resistance, and the F_{60} value under 12.84×10^4 times load repetitions as the evaluation indicator for the long-term skid-resistance, and the BPN* value of pavement under 1 mm water film thickness (BPN^*_{1mm}), the skid-resistance attenuation percentage of pavements under 0.1 mm water film thickness ($F_{0.1}$), the minimum BPN* value of pavements under the partial-covered ice situation (BPN^*_{min}), and the maximum

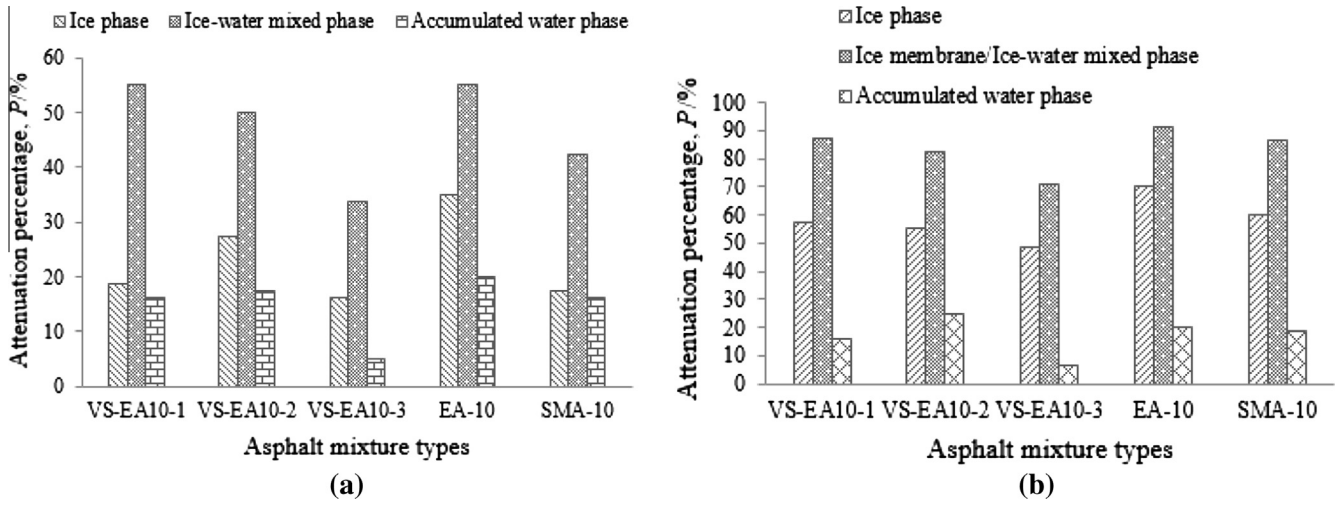

Fig. 23. The skid-resistance attenuation percentages of pavements under different ice situations. (a) Partial-covered ice situation (b) All-covered ice situation.

Table 13
Skid-resistance indicator values of different pavements.

Asphalt mixture types	VS-EA10-1	VS-EA10-2	VS-EA10-3	EA-10	SMA-10
BPN	66	62	76	65	67
MTD (mm)	0.98	1.08	1.14	0.21	0.94
F_{60}	0.291	0.286	0.375	0.028	0.192
BPN^*_{1mm}	64	61	75	60	65
$F_{0.1}$ (%)	8.75	5.33	10.99	18.07	13.75
$BPN^*_{\min}$	36	40	52	35	45
$P_{\max}$ (%)	55.0	46.7	41.8	56.6	42.5

skid-resistance attenuation percentage of pavements under the partial-covered ice situation ($P_{\max}$) were chosen as the evaluation indicators for the skid-resistance under the inclement weather condition. These indicator values of different pavements are summarized in Table 13.

The gray correlation analysis is a comprehensive evaluation method studying the relationship between various factors of gray system [24]. The steps are summarized below.

(1) Determination of original reference sequence, X_0 and original compare sequence, X_i
The optimum data series of the things to be evaluated form the reference sequence while its impact factor data series form the compare sequence.

$$X_0 = \{x_0(1),\ x_0(2),\ldots,x_0(n)\} \tag{11}$$

$$X_i = \{x_i(1),\ x_i(2),\ldots,x_i(n)\} \tag{12}$$

(2) Homogenization treatment of the dimensionless reference sequence and compare sequence

$$Y_0 = \{y_0(1),y_0(2),\ldots,y_0(n)\},\left(y_0(k) = \frac{x_0(k)}{\frac{1}{n}\sum_{k=1}^{n} x_0(k)}, k = 1,2\ldots n\right) \tag{13}$$

$$Y_i = \{y_i(1),y_i(2),\ldots,y_i(n)\},\left(y_i(k) = \frac{x_i(k)}{\frac{1}{n}\sum_{k=1}^{n} x_i(k)}, k = 1,2\ldots n\right) \tag{14}$$

(3) Initialization treatment of the dimensionless reference sequence and compare sequence

Table 14
Calculation of the correlation degree.

	VS-EA10-1	VS-EA10-2	VS-EA10-3	EA-10	SMA-10
S_0	1.336	1.336	1.336	1.336	1.336
S_i	0.861	0.847	1.152	2.361	0.538
$S_i - S_0$	0.860	0.808	0.184	3.698	1.411
ε_{0i}	0.788	0.797	0.950	0.560	0.671

$$Y_0^0 = (y_0^0(1),y_0^0(2),\ldots,y_0^0(n)),\quad (y_0^0(k) = y_0(k) - y_0(1)) \tag{15}$$

$$Y_i^0 = (y_i^0(1),y_i^0(2),\ldots,y_i^0(n)),\quad (y_i^0(k) = y_i(k) - y_i(1)) \tag{16}$$

(4) Calculating the correlation degree

$$s_0 = \sum_{k=2}^{n-1}|y_0^0(k)| + \frac{1}{2}|y_0^0(n)|,\quad s_i = \sum_{k=2}^{n-1}|y_i^0(k)| + \frac{1}{2}|y_i^0(n)| \tag{17}$$

$$s_i - s_0 = \sum_{k=2}^{n-1}|y_i^0(k) - y_0^0(k)| + \frac{1}{2}|y_i^0(n) - y_0^0(n)| \tag{18}$$

$$\varepsilon_{0i} = \frac{1 + |s_0| + |s_i|}{1 + |s_0| + |s_i| + |s_i - s_0|} \tag{19}$$

where ε_{0i} is the gray correlation degree between X_0 and X_i, the larger value of ε_{0i} indicates a higher similarity between X_0 and X_i. The calculation process and results are listed in Table 14. It can be seen that the correlation degree ranking of different asphalt mixtures is: VS-EA10-3 > VS-EA10-2 > VS-EA10-1 > SMA-10 > EA-10. The result shows that

VS-EA10 has the better comprehensive skid-resistance than SMA-10 and EA-10. In addition, the VS-EA10-3 has the first-rank comprehensive skid-resistance, then following the VS-EA10-2 and VS-EA10-1. Therefore, when designing the VS-EA10, the recommended value of the fine aggregate gradation design parameter, n (as shown in Eq. (4)), is restricted to the scope of 0.20 to 0.30, and the VS-EA10 with better skid-resistance could be designed through increasing the value of n.

5. Conclusions

This paper designed the skeleton-dense epoxy asphalt mixture based on the V-S design method, and evaluated the skid-resistance of the novel epoxy asphalt mixture. Results of this study can be summarized as follows.

(1) The designed VS-EA10 could meet the operating requirements of steel bridge pavement, and the VS-EA10 has superior high-temperature stability and anti-fatigue performance, but the deformability of VS-EA10 at low temperature needs to be improved.
(2) The designed VS-EA10 could vastly increase the initial skid-resistance of EAM, and the VS-EA10-3 has the first-rank initial skid-resistance.
(3) The skid-resistance durability of VS-EA10 is dramatically superior to SMA-10, and VS-EA10-3 has the longest skid-resistance life, then followed VS-EA10-1 and VS-EA10-2.
(4) The skid-resistance of VS-EA10-1 and VS-EA10-2 under the rainy condition are comparable to that of SMA-10, and are slightly better than that of EA-10, while the VS-EA10-3 has a dramatically superior skid-resistance than the EA-10 and SMA-10 under the rainy condition. In addition, the skid-resistance attenuations of VS-EA10 are slightly better than that of SMA-10, and much better than that of EA-10.
(5) The minimum skid-resistance and the skid-resistance attenuations of VS-EA10 and SMA-10 in the freezing day are superior to that of EA-10, and VS-EA10-3 has the best skid-resistance in the freezing day.
(6) According to the gray correlation analysis result, VS-EA10 has the better comprehensive skid-resistance than SMA-10 and EA-10. When designing the VS-EA10, the recommended value of fine aggregate gradation design parameter, n, is restricted to the scope of 0.20 to 0.30, and the VS-EA10 with better skid-resistance could be designed through increasing the value of n.

Acknowledgments

This study was supported by the National Natural Science Foundation of China(No. 51378122).

Reference

[1] W. Huang, Z.D. Qian, G. Chen, Epoxy asphalt concrete paving on the deck of long-span steel bridge [J], Chin. Sci. Bull. 48 (21) (2003) 2391–2394.
[2] R. Gaul, A long life pavement for orthotropic bridge decks in China, in: Proceedings of Selected Papers from the 2009 Geohunan International Conference, 2009.
[3] Luo Sang, Qian Zhendong, Experimental research on surface characteristics of epoxy asphalt concrete pavement [J], J. Beijing Univ. Technol. 38 (2) (2012) 219–222 (in Chinese).
[4] Zhang Xiaoning, Zhang Shunxian, Xu Wei, et al., Application performance-based design of epoxy asphalt concrete applied to steel bridge deck pavement [J], J. South Chin. Univ. Technol. (Nat. Sci. Ed.) 40 (7) (2012) 1–7 (in Chinese).
[5] M. Akihiro, J. Toshiro, N. Takaaki, et al., Construction and pavement properties after seven years in porous asphalt with long life [J], Constr. Build. Mater. 50 (2014) 401–413.
[6] Li. Rui, Li. Yanwei, Shi. Xin, et al., Design of small stone asphalt mixture based on anti-skidding performance [J], J. Wuhan Univ. Technol.-Mater. Sci. Ed. 27 (4) (2012) 789–793.
[7] J. Motter, L. Miranda, L. Bernucci, Performance of hot mix asphalt concrete produced with coarse recycled concrete produced with coarse recycled concrete aggregate [J], J. Mater. Civ. Eng. 27 (11) (2015) 04015030.
[8] H.B. Takallou, H.U. Bahia, D. Perdomo, R. Schwartz, Use of superpave technology for design and construction of rubberized asphalt mixtures [C], Transp. Res. Rec. 1583 (1997) 71–87.
[9] Yongli. Zhao, Xu. Tao, Xiaoming. Huang, Zhidong. Li, Gradation design of the aggregate skeleton in asphalt mixture [J], J. Test. Eval. 40 (7) (2012) 1–6.
[10] Dong. Zhang, Xiaoming Huang, Yongli Zhao, Sulong Zhang, Rubberized asphalt mixture design using a theoretical model [J], Constr. Build. Mater. 67 (2014) 265–269.
[11] Ministry of Transport of P.R. China, JTG E42-2005: Test Method of Aggregate for Highway Engineering, China Communications Press, Beijing, 2005.
[12] ASTM D638-10, standard test method for tensile properties of plastics, 2003.
[13] Ministry of Transport of P.R. China, JTG E20-2011: Highway Engineering Asphalt and Asphalt Mixture Testing Procedures, China Communications Press, Beijing, 2011.
[14] Wang Fuyu, The Design and Construction of SAC13 Asphalt Mixture Doctoral Thesis, Jilin University, 2007 (in Chinese).
[15] Ma Baoguo, Study on mixture design method of stone matrix asphalt pavement based on skid resistance Master Thesis, Chang'an University, 2012 (in Chinese).
[16] ASTM E965-96, Standard test method for measuring pavement macrotexture depth using a volumetric technique, 2006.
[17] Ministry of Transport of P.R. China, JTG E60-2008: Field Test Methods of Subgrade and Pavement for Highway Engineering, China Communications Press, Beijing, 2008.
[18] ASTM E303-93, Standard test method for measuring surface frictional properties using the British pendulum tester, 2013.
[19] P. Cao, X. Yan, X. Bai, C. Yuan, Effects of contaminants on skid resistance of asphalt pavements, Traffic Transp. Stud. (2010) 1341–1351.
[20] M.T. Do, V. Cerezo, H. Zahouani, Laboratory test to evaluate the effect of contaminants on road skid resistance [J], J. Eng. Tribol. 228 (11) (2014) 1276–1284.
[21] D. Wang, X. Xie, M. Oeser, B. Steinauer, Simulation and evaluation of the seasonal evolution of the skid resistance on asphalt surfaces using aachen polishing machine [J], Airfield Highway Pavements (2015) 306–317.
[22] J. Doyle, I. Howard, Laboratory assessment of skid resistance for high RAP content warm mixed asphalt, Geo-Frontiers (2011) 4515–4524.
[23] PIARC World Road Association, International PIARC experiment to compare and harmonize texture and skid resistance measurements Rep., PIARC Technical Committee on Surface Characteristics, Paris and Madrid, 1995a.
[24] Z. Chen, K. Zhang, Research on linkage development between manufacturing and logistics industry-based on gray correlation analysis, ICLEM 2010 (2010) 562–568.